

Tunable polariton absorption of distributed feedback microcavities at room temperature

Tohru Fujita, Yoshihiro Sato, Tetsuya Kuitani, and Teruya Ishihara*

Department of Physical Electronics, Faculty of Engineering, Hiroshima University, 1-4-1 Kagamiyama, Higashi-Hiroshima 739, Japan

(Received 13 November 1997; revised manuscript received 21 January 1998)

We have demonstrated well-separated tunable polariton absorption for a semiconductor-cavity composite system in transmission measurements at room temperature. A distributed feedback microcavity of the fourth order is fabricated by spin coating a self-organized inorganic/organic multiple quantum wells, $(\text{C}_6\text{H}_5\text{C}_2\text{H}_4\text{NH}_3)_2\text{PbI}_4$, on a corrugated quartz substrate with a period of about $0.7 \mu\text{m}$. By changing the grating period or the incident angle, the absorption dips exhibit anticrossing behavior. Owing to the large excitonic oscillator strength of the material, the polariton mode splitting is as large as 100 meV even at room temperature. At the normal incidence, an exciton and a light form a strongly coupled standing wave, which corresponds to a cavity polariton in Fabry-Perot semiconductor microcavities. [S0163-1829(98)10719-1]

I. INTRODUCTION

Owing to the recent development of crystal growth and nanofabrication techniques, we are now beginning to control the spontaneous and stimulated emissions with microcavities^{1,2} and/or photonic crystals,³ the structure of which is characterized by the size of the light wavelength. Just as the exciton energy is controlled by the quantum-well thickness, so too can the absorption energy and the coupling coefficient be tuned by the microcavity design. These techniques may be employed to understand fundamental physics of photon-matter interaction, and may be applicable to energy-effective, high-speed light emitters and nonlinear optical switches.

Until recently, however, most of the research has been in the weak-coupling regime, where the photon-matter interaction is treated as a perturbation to the uncoupled system. The strong-coupling regime was first reported by Weisbuch *et al.*⁴ in 1992 for GaAs quantum wells (QW's) in a Fabry-Perot (FP) microcavity; they observed two reflection dips exhibiting anticrossing behavior as the cavity length changes, and interpreted it in terms of strongly coupled states of an exciton and a photon in the cavity, or upper and lower cavity polaritons. So far the largest polariton splitting energy observed in such a system is 9 meV for III-V,⁵ and 18 meV for II-VI compounds,⁶ which seems to be too small to be applied for device operations at room temperature. Therefore one needs to choose a material with large excitonic oscillator strength, and then an appropriate microcavity for it. Although FP microcavities have been commonly utilized, distributed feedback (DFB) cavities may open new possibilities for application. These two types of cavities can be related through a Fourier transformation in space; still, it is intriguing to investigate polaritons in a DFB cavity in its own right. There are few works for polaritons in DFB cavities; Kohl *et al.*⁷ etched GaAs QW samples to form periodic structure in order to observe photoluminescence from the quantum-well-exciton polaritons. From a theoretical point of view, Tassone and Bassani,⁸ and Citrin⁹ discussed the (weak) coupling between the electromagnetic field and one-dimensional exciton wires in the grating structures.

In this paper, we will report on the DFB cavity polariton absorption at room temperature for a semiconductor with large oscillator strength. The paper is organized as follows. After describing the sample structures in Sec. II, we discuss what we expect in the experiments in Sec. III. Then we show transmission spectra under several conditions on the grating pitch, incident angle, and polarization in Sec. IV, which support the existence of polaritons at room temperature. In Sec. V, we analyze the origin of polariton splitting for DFB and FP microcavities. Finally, in Sec. VI we summarize our results and conclude. A preliminary result has been reported in Ref. 10.

II. SAMPLES

The structure of our DFB microcavity is schematically shown in Fig. 1. This DFB cavity consists of quartz grating substrate, an active material, and an overcoating film. The grating was fabricated on a quartz substrate by means of the electron-beam lithography and dry etching techniques. In order to dissipate electric charge accumulation at exposure, we spin coated an electrically conducting film on a negative-type resist film. Typical grating pitch (Λ), depth (h), line and space ratio (L - S ratio), and area are $0.7 \mu\text{m}$, $0.3 \mu\text{m}$, 1:4, and $1.5 \text{ mm} \times 1.5 \text{ mm}$, respectively. The active material we used is $(\text{C}_6\text{H}_5\text{C}_2\text{H}_4\text{NH}_3)_2\text{PbI}_4$ [bis-(phenethylammonium) tetraiodoplumbate (PEPI)] which is one of the PbI_4 -based layered perovskite-type semiconductors. PbI_4 -based layered perovskite-type semiconductors have

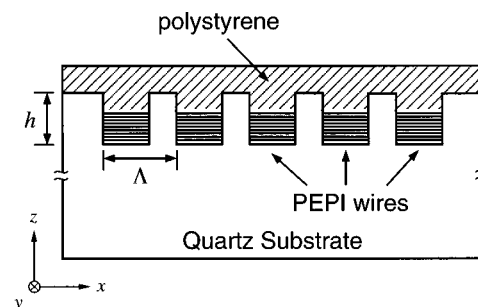


FIG. 1. Structure of a DFB microcavity (not to scale).

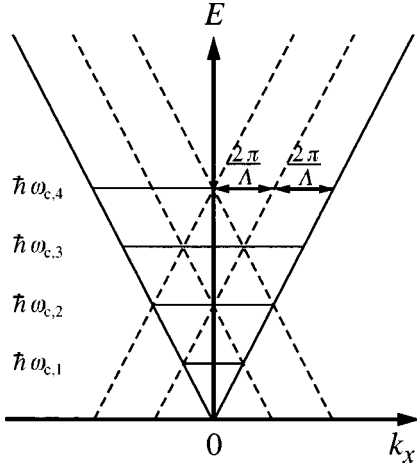


FIG. 2. Schematic dispersion relations of light propagating along a film on the periodic substrate (solid lines) and their replicas (dashed lines). The guided-wave dispersion is neglected in the figure for simplicity. $\hbar\omega_{c,m}$ are the m th-order cavity resonance energies.

self-organized multiple quantum-well structure with the $[\text{PbI}_6]^{4-}$ layers as wells and organic alkylammonium layers as barriers. Electron-hole pairs in the well combine strongly owing to the image charge effect by virtue of the large difference in dielectric constants between the wells and the barriers (for example, $\epsilon_{\text{well}}=6.1$, $\epsilon_{\text{barrier}}=3.22$ in PEPI). In PEPI, therefore, exciton binding energy, oscillator strength, and L - T splitting are enormous: 220 meV, 0.5 per formula unit, and 50 meV, respectively.¹¹ Another benefit of these materials is that a high-quality polycrystalline film on a substrate can be easily obtained by spin coating its organic solution. The c axes of polycrystallines in a film are aligned to be perpendicular to the substrate plane. In the present experiments, we formed 0.03- μm -thick PEPI film in the grooves of gratings by spin coating a solution of PEPI in dimethylsulfoxide, 80 mg/ml, at 6000 rpm. The sample thus prepared can be regarded as an array of semiconductor wires. Finally, we overcoat a 0.5- μm -thick polystyrene in xylene at 6000 rpm in order to keep the PEPI film away from oxygen and moisture. The polystyrene film not only prevents PEPI from degradation but also plays as an important role as forming a waveguide, as will be mentioned later (see Sec. V C below). We formed six gratings on a quartz substrate with grating pitch Λ ranging from 0.62 μm to 0.72 μm every 20 nm, so that we can compare their transmission spectra under the same conditions.

III. PRELIMINARY DISCUSSION

Transmitted intensity of a light through the sample is measured as a function of the photon energy in our experiments. Let us fix the Cartesian coordinate so that the direction of the grating lines and the normal of the substrate are the y and z axes, respectively. The x axis is the direction of the periodic modification.

Figure 2 represents schematic dispersion relations for the polystyrene waveguide structure on a grating substrate. By virtue of the reciprocal lattice vector,

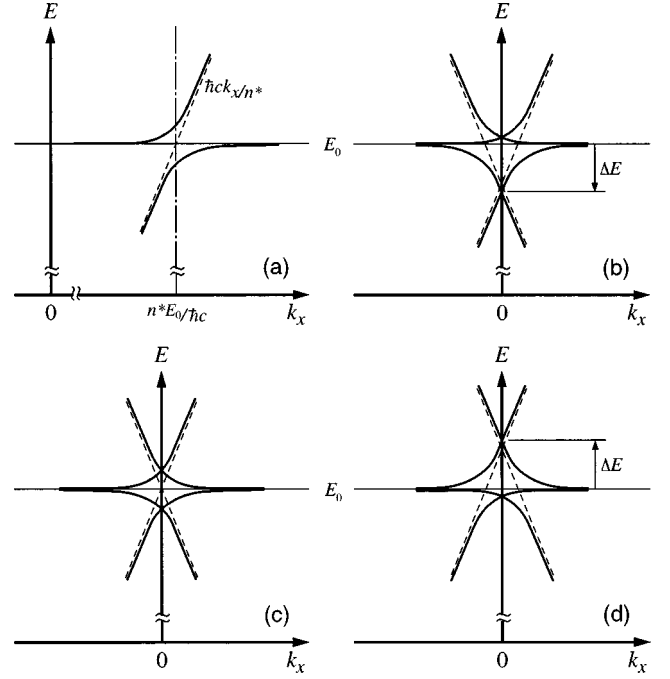


FIG. 3. Schematic polariton dispersion relations in a DFB microcavity (a) near $k_x = n^*E_0/\hbar c$ and near $k_x = 0$ for (b) $\Delta E < 0$, (c) $\Delta E = 0$, and (d) $\Delta E > 0$, respectively. The solid lines are polariton dispersion curves, and the dashed and thin lines are the uncoupled guided-wave and exciton dispersion curves, respectively.

$$G_m = \frac{2\pi}{\Lambda} m, \quad \text{where } m \text{ is an integer,} \quad (1)$$

the original dispersion curves (solid lines) are folded to form replicas (dashed lines). An optical standing wave is formed at the photon energy that satisfies $k_x - (-k_x) = G_m$. Let us refer this energy to the m th-order cavity resonance energy hereafter:

$$\hbar\omega_{c,m} = \frac{\pi\hbar c}{n^*\Lambda} m, \quad (2)$$

where $n^* = ck_x/\omega$ is the effective index of refraction for the waveguide.

When a thin PEPI film is inserted between the polystyrene film and the grating substrate, an exciton in the PEPI layer strongly couples to the guided-wave mode to form polaritons as is schematically shown in Fig. 3(a). When $\Lambda \sim 0.7 \mu\text{m}$, the fourth-order cavity resonance energy falls near the exciton energy $E_0 = 2.4 \text{ eV}$; then $G_{\pm 2}$ brings the polariton anti-crossing region into the light cone, which is accessible by the light in the free space. In Figs. 3(b)–3(d), the polariton dispersions folded into $k_x \sim 0$ are shown for (b) $\Delta E < 0$, (c) $\Delta E = 0$, and (d) $\Delta E > 0$, respectively. The detuning energy is defined as $\Delta E = \hbar\omega_{c,4} - E_0$. When the incident beam is tilted to the x direction by an angle θ , it excites the guided-wave mode with $k_x = k \sin \theta$, causing intensity loss in the transmission spectrum at the corresponding energy. Thus we can determine the dispersion curves experimentally. At $k_x = 0$, the strongly coupled states are formed between an optical standing wave and an exciton in the DFB microcavities. Since these states are analogous to the cavity polaritons in FP mi-

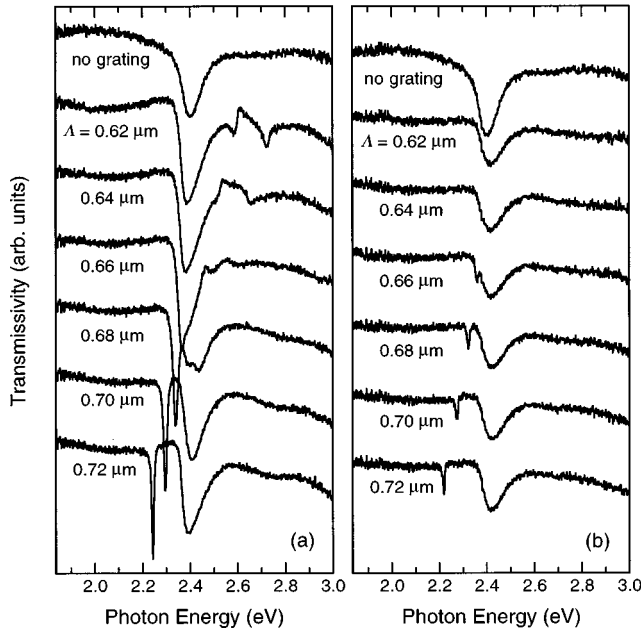


FIG. 4. Transmission spectra of samples at 300 K for normal incidence. The polarization of the incident light is (a) $\mathbf{E} \perp \hat{\mathbf{x}}$ and (b) $\mathbf{E} \perp \hat{\mathbf{y}}$. The topmost spectra are for PEPI on a quartz substrate without grating structure. The lower spectra are for PEPI film on a grating with pitches of $\Lambda = 0.62, 0.64, 0.66, 0.68, 0.70,$ and $0.72 \mu\text{m}$, respectively.

crocavities, we may call them ‘‘DFB cavity polaritons.’’ The coupling is the strongest when the cavity resonance energy coincides with the exciton absorption energy as shown in Fig. 3(c). In the DFB microcavities, we can observe the states with finite k_x (i.e., the states propagating along the cavity axis), to which there are no correspondences in the FP microcavities.

IV. RESULTS

A. Normal incidence

Figure 4 shows the transmission spectra for normal incidence of the DFB cavities with $\Lambda = 0.62, 0.64, 0.66, 0.68, 0.70,$ and $0.72 \mu\text{m}$, respectively. The polarization of the incident light is $\mathbf{E} \perp \hat{\mathbf{x}}$ and $\mathbf{E} \perp \hat{\mathbf{y}}$ in Figs. 4(a) and 4(b), respectively. On the top in Fig. 4(a) and 4(b), we also show transmission spectra of a PEPI film on a quartz substrate without cavity as a reference. First, we look at the spectrum for $\Lambda = 0.72 \mu\text{m}$; the broad absorption band near 2.4 eV is ascribed to the lowest exciton of PEPI, and is mainly (about 3:1) polarized to the grating grooves. Since it is also observable for the film on a plain substrate, we call this dip the excitonlike mode. On the other hand, the sharp dip at 2.24 eV is observable only with the DFB cavity. We refer this sharp dip to a cavitylike mode. As Λ decreases, the cavitylike mode shifts to the higher energies, broadens, and eventually connects to the broad dip at 2.4 eV for $\Lambda = 0.62 \mu\text{m}$. Simultaneously, a broad dip at 2.4 eV for $\Lambda = 0.72 \mu\text{m}$ shifts to the higher energies, and connects to the sharp dip at 2.58 eV for $\Lambda = 0.62 \mu\text{m}$. For shorter Λ 's ($\Lambda = 0.66, 0.64,$ and $0.62 \mu\text{m}$) in Fig. 4(a), we can see two

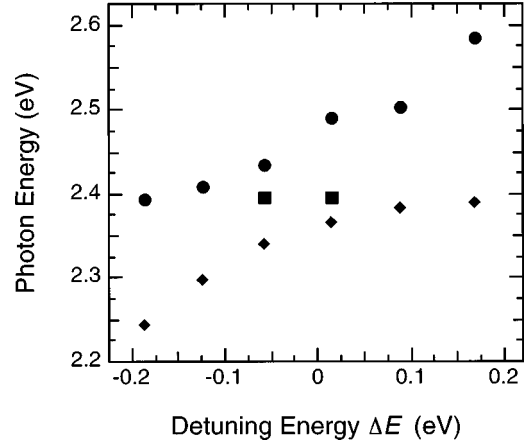


FIG. 5. Transmission dip positions in normal-incidence transmission spectra for $\mathbf{E} \perp \hat{\mathbf{x}}$ as a function of cavity detuning energy. Dips due to the higher-order transverse modes are omitted for simplicity. Closed circles and diamonds correspond to the upper and lower branches of a DFB cavity polariton, respectively. Closed squares correspond to the absorption of the upper branch polaritons not affected by the reciprocal lattice vectors.

cavitylike modes. These are ascribed to the lowest and next-higher order transverse modes in the waveguide (see Sec. V C below).

Figure 5 reproduces the positions of the dips in Fig. 4(a) as a function of ΔE . Dips due to the higher-order transverse modes are omitted for simplicity. In Fig. 5, we see that these dips exhibit the anticrossing behavior between exciton and cavity modes, which is similar to the cavity polariton dispersion observed in the FP microcavity. This behavior demonstrates that a guided-wave mode couples to an exciton so strongly that they form new eigenstates, which we refer to as DFB cavity polaritons. Closed circles and lozenges in Fig. 5 correspond to the upper and lower branch of the DFB cavity polaritons, respectively. The mode splitting at resonance is 100 meV, which is much larger than 9 meV observed in the GaAs system's. This is ascribed to the large excitonic oscillator strength of PEPI. The polariton splitting could be larger than the one observed here, because the electric-field confinement factor was not optimized in the present experiments.

The small dips between the upper and the lower branches are plotted as closed squares in Fig. 5. They may be ascribed to the transition to the bottom of the ‘‘original’’ upper branch polaritons, which were not affected by the reciprocal lattice vectors. For polarization $\mathbf{E} \perp \hat{\mathbf{y}}$, we did not find the mode splitting between the upper and lower polariton modes in this particular sample. Therefore we will show the results only for the polarization of $\mathbf{E} \perp \hat{\mathbf{x}}$ hereafter.

B. k_x dependence

Next, we show the θ dependence of the transmission spectra, with which we can investigate the coupling states with finite k_x (i.e., the polariton propagating along to the cavity axis). Figure 6 shows the transmission spectra for $\Lambda = 0.72 \mu\text{m}$ for several θ 's ranging from 0° to 15° . The polarization of the incident light is parallel to the grating

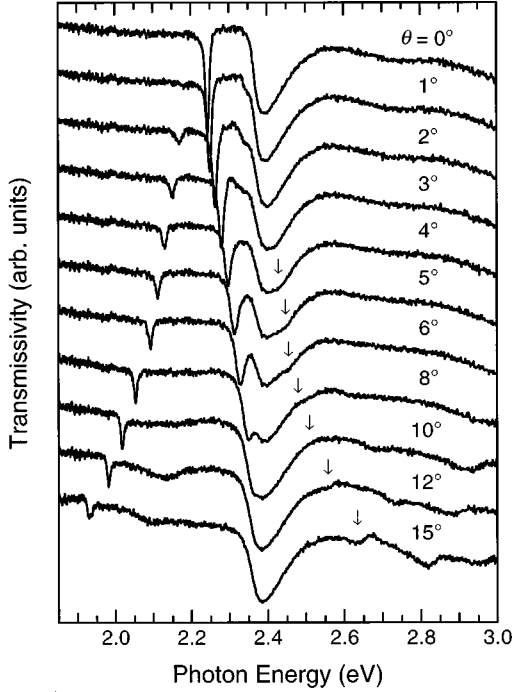


FIG. 6. Transmission spectra ($\Lambda=0.72 \mu\text{m}$) for several θ 's, ranging from 0° to 15° . The polarization of the incident light is $\mathbf{E} \perp \hat{\mathbf{x}}$.

line, $\mathbf{E} \perp \hat{\mathbf{x}}$. For $\theta=0^\circ$ ($k_x=0$), we observe only one cavity dip. As the angle θ increases, we observe that the dip splits into two; one shifts to the higher energies and the other shifts to the lower energies. We call these modes the guided-wave-like modes. When the blueshifting mode approaches the PEPI's exciton absorption band at around $\theta=5^\circ$, the shift saturates and approaches the exciton absorption peak asymptotically. Simultaneously, a small dip marked by an arrow in Fig. 6 shifts to higher energies as θ increases. This dip is attributed to the upper branch polariton mode. All dips on the spectra are plotted in Fig. 7(a) as a function of k_x . Also shown in Fig. 7 are the results for (b) $\Lambda=0.68 \mu\text{m}$ and (c) $0.62 \mu\text{m}$. These are the experimental results that should be compared to Figs. 3(b)–3(d); we conclude that the dips we observed are readily ascribed to the well-defined polariton at room temperature.

In our measurements, the transmission dips tend to smear at 2.4–2.5 eV. This may be ascribed to the fact that the effective grating area is small because of the large absorption. In Fig. 7(a), it is clearly seen that the exciton and the guided-wave-like modes anticross near $k_x = \pm 0.15 \times 10^5 \text{ cm}^{-1}$ (see the region marked by circles). This guided-wave polariton splitting is again 100 meV.

Although two dispersion curves cross at $k_x=0$ in the schematic figure, Fig. 3, the experimental data exhibit a gap of about 50 meV below exciton absorption. This gap corresponds to the so-called photonic band gap (PBG) and will be discussed in Sec. V B.

C. k_y dependence

When the incident beam is tilted to the y direction by an angle α , it excites the guided-wave mode with (k_x, k_y)

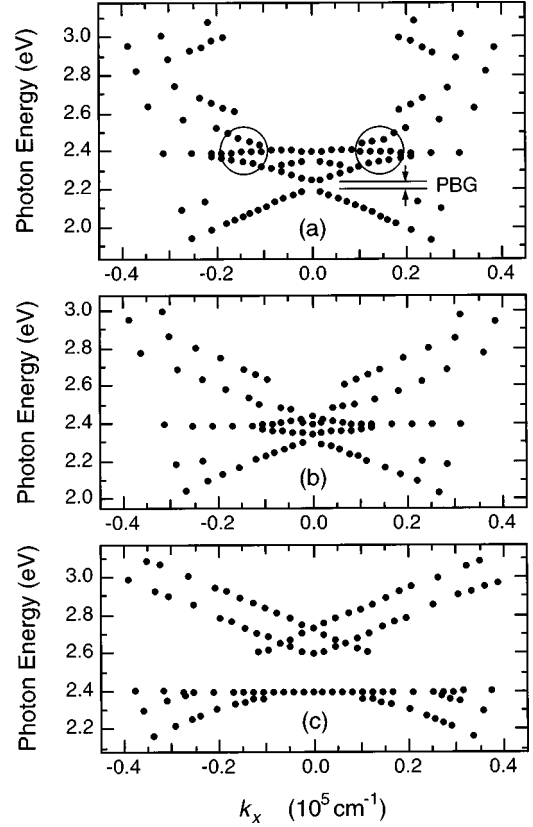


FIG. 7. Transmission dip energy as a function of k_x for (a) $\Lambda=0.72 \mu\text{m}$, (b) $\Lambda=0.68 \mu\text{m}$, and (c) $\Lambda=0.62 \mu\text{m}$.

$=(0, k \sin \alpha)$. Because the wave thus excited is always a standing wave in the x direction, it is equivalent to tilting an incident-angle in a FP microcavity.¹² Neglecting the polariton and the waveguide effects, the angular frequency of the cavity-resonance mode is given by

$$\omega = \frac{c}{n^*} \sqrt{\left(m \frac{2\pi}{\Lambda}\right)^2 + (k \sin \alpha)^2}, \quad (3)$$

where c is the light velocity in vacuum. When that cavity mode approaches the exciton band, the dispersion curves are expected to exhibit an anticrossing behavior (the polariton splitting). Figure 8 shows the α dependence of the transmission spectra for $\Lambda=0.7 \mu\text{m}$. The polarization of the incident light is again $\mathbf{E} \perp \hat{\mathbf{x}}$. We find that a cavitylike mode located at 2.3 eV at $\theta=\alpha=0^\circ$ shifts to the higher-energy side as increasing the angle α . The dip seen for $19^\circ < \alpha < 30^\circ$ at 2.4 eV may be ascribed to the absorption of the upper branch polariton, which is not affected by the reciprocal lattice vectors as mentioned earlier. The dips are reproduced in Fig. 9(a) as a function of k_y . The results for $\Lambda=0.72 \mu\text{m}$ are shown in Fig. 9(b). They demonstrate clearly that the dispersion curves exhibit the polariton splitting. In both cases, the mode splittings are again about 100 meV. Thus we observed a nearly equal amount of splitting in the Λ , the k_x , and k_y dependences of the absorption dip energy. This is reasonable, because in these experiments we are observing the ‘‘replica’’ of the guided-wave polaritons via the reciprocal lattice vectors.

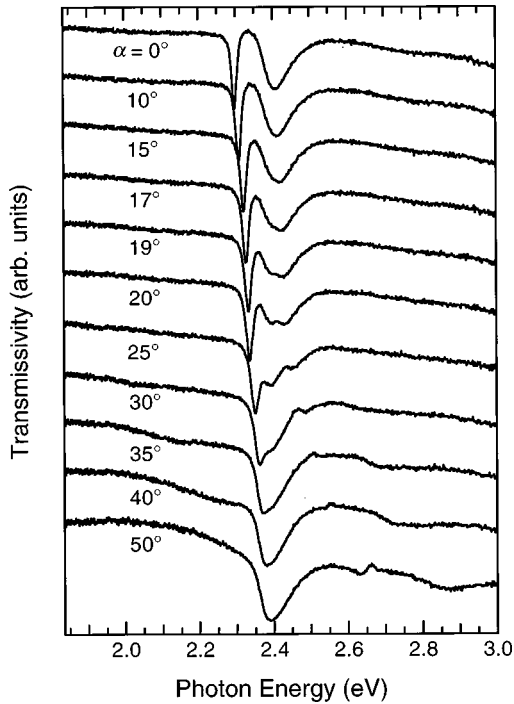


FIG. 8. Transmission spectra ($\Lambda=0.70 \mu\text{m}$) for several α 's, ranging from 0° to 50° . The polarization of the incident light is $\mathbf{E} \perp \hat{\mathbf{x}}$.

V. DISCUSSION

In this section, we first compare the polariton in our DFB microcavities with the one in FP microcavities, then we discuss the polarization dependence. Finally we give some comments on the DFB cavity structure.

A. Polariton splitting in DFB and FP microcavities

As mentioned above, the polariton splitting of PEPI film in our DFB cavity is about 100 meV. Although this value is much larger than 9 meV observed in GaAs quantum wells embedded in the FP microcavity, it is not as large as ex-

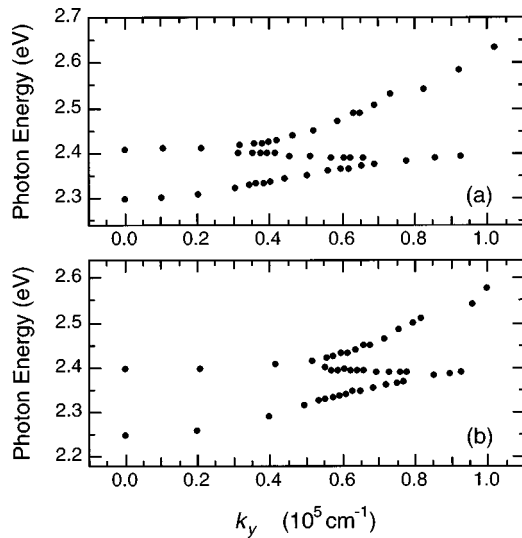


FIG. 9. Transmission dip energy as a function of k_y for (a) $\Lambda=0.70 \mu\text{m}$ and (b) $\Lambda=0.72 \mu\text{m}$.

pected from the large oscillator strength of the exciton in PEPI. Here, we will consider the reason. The polariton splitting, which is often referred to vacuum Rabi splitting,⁴ is the energy difference between two eigenmodes that occur under the strong coupling between an oscillator (exciton or atom) state and a photon state. In bulk semiconductor crystals, the polariton splitting energy is defined for each wave vector. For the resonant wave vector,

$$\hbar \omega_{\text{PS}} = \sqrt{2 \hbar \omega_0 \Delta_{\text{LT}}}, \quad (4)$$

where Δ_{LT} is the longitudinal-transverse splitting energy in a bulk crystal, which is proportional to the excitonic oscillator strength per unit volume, and $\hbar \omega_0$ is the transverse exciton energy. As the crystal thickness becomes shorter, the photon mode in the crystal becomes more discrete. But since this is nothing more than selecting a wave vector from the continuous dispersion in bulk, the magnitude of the polariton splitting in thin crystals is identical to the one in bulk. When the thickness is comparable to the wavelength, it is analogous to a semiconductor FP microcavity. In reality, the active material does not fill the cavity, and the magnitude of the splitting depends on the thickness and the location of the active material. Now, it is clear that the splitting never exceeds the one in bulk, except for the enhancement of the oscillator strength owing to the quantum size effect. In other words, we must use a material with a large excitonic oscillator strength per unit volume in order to realize a large polariton splitting. Actually, by substituting appropriate parameters in the GaAs systems into Eq. (4), we can obtain the cavity polariton splitting observed experimentally. A similar discussion has been given by Andreani *et al.*¹³ The same is true in the DFB microcavity, which can be seen as a periodically filled bulk crystal; the splitting energy is determined by an overlapping integral of PEPI wires and the optical field, which depends on a width of the grating and a thickness of PEPI film, and is never larger than the one in bulk. The splitting energy is estimated from Eq. (4) to be 500 meV for a PEPI bulk crystal, and the observed one in our DFB cavity is only 20% of it. It means that the confinement factor of the wave guide is about 20%, which is reasonable if the ratio of the dielectric constant in the waveguide and the thickness of the film are taken into account. Generally speaking, $\hbar \omega_{\text{PS}}$ can be reduced by the exciton damping energy Γ :

$$\hbar \omega'_{\text{PS}} = \hbar \omega_{\text{PS}} \sqrt{1 - (\Gamma/\hbar \omega_{\text{PS}})^2}. \quad (5)$$

Estimating Γ from the absorption width, we find that this correction is negligible in the present case.

B. Polarization dependence

Now we discuss some polarization dependences in our experimental results. Note that the electromagnetic field propagating along the x direction is modified by the periodic structure. Therefore, we observe a transverse electric (TE) mode for the $\mathbf{E} \perp \hat{\mathbf{x}}$ polarization of the incident light and transverse magnetic (TM) mode for $\mathbf{E} \perp \hat{\mathbf{y}}$ in the normal-incidence and the finite θ measurements. In the case of finite α , TE and TM modes are mixed.

We first give our attention to the depth of the transmission dips. The dip due to TE mode is more than twice as deep as

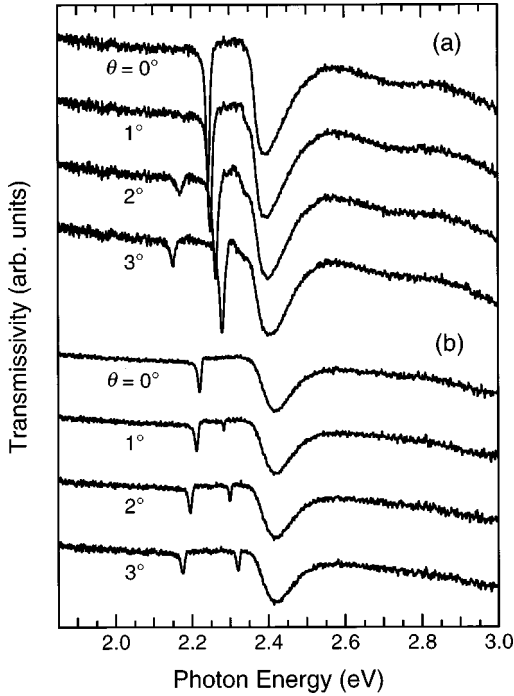


FIG. 10. Transmission spectra ($\Lambda=0.72 \mu\text{m}$) at small θ 's for (a) $\mathbf{E} \perp \hat{\mathbf{x}}$ and (b) $\mathbf{E} \perp \hat{\mathbf{y}}$ polarization.

the one due to TM mode. We have confirmed that the exciton absorption does not depend on the polarization for a PEPI film on the substrate without grating structures. The exciton wave function is hardly modified by the confinement effect due to the grating grooves, because its width, $\sim 500 \text{ nm}$, is much larger than the exciton Bohr radius, 1.7 nm . Then let us consider an anisotropic local field induced by the grating structures. When the polarization is perpendicular to the grating lines, $\mathbf{E} \perp \hat{\mathbf{y}}$, it is expected that the local electric field becomes much weaker in the grooves on account of the polarization charges, which results in the smaller absorption. This phenomena has been reported in photoluminescence of an isolated GaAs quantum-well wire and explained by this mechanism.¹⁴

Next, we consider the energy position of the transmission dips, when the cavity resonance locates at lower energy than the exciton absorption. Figure 10 shows the transmission spectra for small θ 's for (a) $\mathbf{E} \perp \hat{\mathbf{x}}$ and (b) $\mathbf{E} \perp \hat{\mathbf{y}}$ polarization for $\Lambda=0.72 \mu\text{m}$. The excitonlike dip locates lower in energy for $\mathbf{E} \perp \hat{\mathbf{x}}$ than $\mathbf{E} \perp \hat{\mathbf{y}}$, which has not been observed in the isolated GaAs quantum-well wire system mentioned above. Then it is necessary to bear in mind that we do not observe an exciton itself but a guided-wave polariton. Irrespective of the grating presence, excitons couple to the guided-wave mode and form the TE or TM guided-wave polaritons. Since the refractive index is larger in the TE mode than the TM one, the dispersion of the guided-wave mode is less steep for the former. By introducing the periodic structures, the dispersion curves are folded; the crossing point of the upper branch dispersion curves at $k_x=0$ should locate at lower energy for the TE mode than the TM one. When we compare $\theta=0^\circ$ spectra for two polarizations, we find that the cavity-like mode, which is originated from the crossing point of the lower branch dispersion, locates at higher energy for the TE

mode than for the TM mode, which at first glance contradicts our argument. We can understand this puzzle by inspecting the transmission spectra for finite θ . As clearly seen in Fig. 10, there is PBG at $\theta=0$ ($k_x=0$); the higher-energy mode (the bottom of the conduction band of PBG) couples only to a photon with $\mathbf{E} \perp \hat{\mathbf{x}}$, while the lower mode (the top of the valence band) couples to a photon with $\mathbf{E} \perp \hat{\mathbf{y}}$. We have confirmed this selection rule by solving the wave equation for the fourth-order cavity resonance and considering the symmetry of the mode, which can couple to photons for two polarizations.

C. Structure dependence

Finally, we give some comments on the cavity structure dependence of the polariton absorption. Our DFB cavity consists of a quartz grating substrate, a PEPI film as an active material and a polystyrene film. The polystyrene film does not only prevent PEPI from degradation but also plays such an important role as forming a waveguide. Actually, if we do not have the polystyrene film, we do not observe a well-defined cavity mode as is observed above. Since the polystyrene film has a refractive index of 1.59, which is larger than those of air and quartz, it serves as a core layer of a slab waveguide with a PEPI film. The thicker the core layer is, the more the electromagnetic field is confined in the core (i.e., the confinement factor becomes larger); we can control the interaction between PEPI's exciton and optical field. In order to confirm the formation of a waveguide, we have carried out the mode calculation for an asymmetric slab waveguide. The refractive index of the clad and the core layer are assumed to be $n_{\text{clad}}=1$ (air) and 1.46 (quartz substrate), and $n_{\text{core}}=1.59$ (neglecting the thin PEPI layer) and a thickness of the core layer is measured by a profile meter to be $0.50 \mu\text{m}$. For simplicity, we neglected a dispersion of the material and fixed the refractive indices as constants. As a result, we have found that the lowest TE and TM modes exist above 0.71 eV and 0.91 eV, respectively. The cutoff energy for the second-lowest modes is 2.68 eV and 2.89 eV, respectively. Thus, in the exciton resonance energy at 2.4 eV, there is only one guided-wave mode for a given polarization. In order to prepare a sample without higher-order transverse modes in the whole spectral range we measured, we could have used a thinner polystyrene film. It is, however, rather difficult to optimize the thickness to have the deep fundamental dips and no higher modes.

In this paper, we have shown the results in the DFB microcavities whose L - S ratio and a depth of the grating's groove are 1:4 and $0.45 \mu\text{m}$, respectively. In this cavity, we did not observe the anticrossing between the exciton and the cavity mode clearly for $\mathbf{E} \perp \hat{\mathbf{y}}$ polarization as was mentioned above. But we have observed the polariton splitting even for that polarization when we used the DFB microcavity, in which case the L - S ratio and the depth of the grating's groove are 1:2 and $0.15 \mu\text{m}$, respectively. This polariton splitting is about 40 meV, which is smaller than 95 meV for $\mathbf{E} \perp \hat{\mathbf{x}}$ polarization in the same cavity. Although the mode splitting for $\mathbf{E} \perp \hat{\mathbf{x}}$ polarization in this $0.15\text{-}\mu\text{m}$ -deep cavity is nearly equal to that in $0.45\text{-}\mu\text{m}$ -deep cavity, the transmission dips due to the DFB cavity polaritons are seen much less

clearly as shown in Fig. 4. Thus, the coupling states change remarkably due to the structure of the DFB cavity. On the other hand, we may utilize this sensitivity to control the coupling strength of an exciton and a photon in a waveguide, as well as that of a polariton and a photon outside. The systematic study of the system will help us to understand the exciton-photon interaction.

VI. CONCLUSION

Both in DFB and FP microcavities, we can modify the cavity resonant energy and the exciton-photon coupling strength by controlling a cavity length. In other words, a polariton can be controlled by modifying boundary conditions of light by these microcavities, just as the electron wave function can be controlled by a potential profile in a semiconductor quantum well. In this paper, we have fabricated the DFB microcavities with semiconductor film, which has a large excitonic oscillator strength. We have observed the strongly coupled exciton-photon states, DFB cavity polaritons, in transmission measurements at room temperature for the first time, to our knowledge. The polariton mode splitting energy at resonance amounts to 100 meV even at room temperature. The maximum of the polariton splitting is restricted by an excitonic oscillator strength of a material

rather than the microcavity effect, except for the quantum size effect. The large polariton splitting we observed reflects a large excitonic oscillator strength of PEPI. The DFB systems can be viewed as a periodic array of resonant emitters. Actually, we have observed a directional emission in space-resolved photoluminescence measurements.¹⁵

We have developed a versatile method for preparing a periodic structure of optical materials. We expect that it can be utilized not only for the fundamental research but also for the new photonic devices.

ACKNOWLEDGMENTS

We are grateful to Professor M. Yamanishi for valuable discussions, and to Y. Sayama and Y. Hamamoto for technical support. The electron-beam lithography and dry etching processes in this experiment were carried out at the Research Center for Nanodevices and Systems, Hiroshima University. This work has been supported by a Grant-in-Aid for Scientific Research on the Priority Area "Mutual Quantum Manipulation on Radiation Field and Matter" from the Ministry of Education, Science and Culture of Japan, and CREST, Core Research for Evolutional Science and Technology, of JST, Japan Science and Technology Corporation.

*Electronic address: terry@ipc.hiroshima-u.ac.jp

¹H. Yokoyama, K. Nishi, T. Anan, H. Yamada, S. D. Brorson, and E. P. Ippen, *Appl. Phys. Lett.* **57**, 2814 (1990).

²T. Yamauchi, Y. Arakawa, and M. Nishioka, *Appl. Phys. Lett.* **58**, 2339 (1991).

³E. Yablonovitch, *Phys. Rev. Lett.* **58**, 2059 (1987).

⁴C. Weisbuch, M. Nishioka, A. Ishikawa, and Y. Arakawa, *Phys. Rev. Lett.* **69**, 3314 (1992).

⁵R. Houdré, R. P. Stanley, U. Oesterle, M. Ilegems, and C. Weisbuch, *Phys. Rev. B* **49**, 16 761 (1994).

⁶P. Kelkar, V. Kozlov, H. Jeon, A. V. Nurmikko, C.-C. Chu, D. C. Grillo, J. Han, C. G. Hua, and R. L. Gunshor, *Phys. Rev. B* **52**, R5491 (1995).

⁷M. Kohl, D. Heitmann, P. Grambow, and K. Ploog, *Phys. Rev. B* **42**, 2941 (1990).

⁸F. Tassone and F. Bassani, *Phys. Rev. B* **51**, 16 973 (1995).

⁹D. S. Citrin, *IEEE J. Quantum Electron.* **29**, 2117 (1993).

¹⁰T. Ishihara, T. Kuitani, Y. Sato, T. Fujita, and M. Yamanishi (unpublished).

¹¹T. Ishihara, in *Optical Properties of Low Dimensional Materials*, edited by T. Ogawa and Y. Kanemitsu (World Scientific, Singapore, 1995), Chap. 6, p. 288.

¹²R. Houdré, C. Weisbuch, R. P. Stanley, U. Oesterle, P. Pellandini, and M. Ilegems, *Phys. Rev. Lett.* **73**, 2043 (1994).

¹³L. C. Andreani, V. Savona, P. Schwendimann, and A. Quattropani, *Superlattices Microstruct.* **15**, 453 (1994).

¹⁴P. Ils, Ch. Gréus, A. Forchel, V. D. Kulakovskii, N. A. Gippius, and S. G. Tikhodeev, *Phys. Rev. B* **51**, 4272 (1995).

¹⁵T. Fujita, T. Ishihara, Y. Sato, and M. Yamanishi, *Technical Digest of the Pacific Rim Conference on Lasers and Electro-Optics, Chiba, Japan, 1997* (IEEE, New York, 1997), p. 41.